Molecular Dynamics Study of Liquid Condensation on Nano-structured Sinusoidal Hybrid Wetting Surfaces

Taskin Mehereen[1, a)], Shorup Chanda[1, b)], Afrina Ayrin Nitu[1, c)], Jubaer Tanjil Jami[1, d)], Rafia Rizwana Rahim[1,2, e)], Md Ashiqur Rahman[1, f)]

Author Affiliations

[1]*Department of Mechanical Engineering, Bangladesh University of Engineering and technology, Dhaka-1000, Bangladesh*

[2]*Oden Institute for Computational Engineering and Sciences, The University of Texas at Austin, Austin, TX-78712*

Author Emails

[a)] taskin2560@gmail.com
[b)] scshorup.chanda@gmail.com
[c)] afrinanitu71@gmail.com
[d)] jamijubaer@gmail.com
[e)] rafia.rizwana.rahim@utexas.edumailto:
[f)] Corresponding author: ashiqurrahman@me.buet.ac.bd

Abstract. Although real surfaces exhibit intricate topologies at the nanoscale, the rough surface consideration is mostly overlooked in the existing literature. Among different correlations that can be used to represent rough surfaces, superimposed sinusoidal functions offer a particularly effective method to model the complexity of real-world surfaces. The present study investigates the influence of sinusoidal surface roughness on the condensation of liquid argon over a hybrid functionally gradient wetting (FGW) surface using molecular dynamics simulations. In the simulation, argon atoms in both liquid and vapor phases are confined between two platinum substrates. The bottom substrate is flat, while the upper substrate's roughness is modeled using superimposed sinusoidal functions, with the study focusing on a FGW surface containing 84% hydrophilic content. The lower substrate's temperature is raised to 130K to induce the evaporation of argon with the system initially at equilibrium at 90K. The upper wall, maintained at 90K, serves as the condensation site. Key metrics of the nanoscale condensation process, such as time-averaged condensation rates, surface heat flux, and total energy per atom, are analyzed. The results show that increased surface area provided by sinusoidal patterns enhances condensation compared to flat surfaces, offering a more accurate representation of how these intricate surface textures contribute to higher condensation rates. Specifically, higher orders of the sinusoidal functions enhance heat transfer more effectively than lower-order ones. Although greater orders allow for better approximation, they are also found to be computationally more expensive. The present work provides a detailed analysis of how intricate nanoscale surface patterns can be modeled through superimposed sinusoidal functions and can be the groundwork for modeling optimized surfaces that achieve superior condensation heat transfer.

INTRODUCTION

The efficient management of thermal energy remains a critical challenge across numerous industries, and various methods of effective heat transfer plays a crucial role in mitigating this issue. From steam powerplants[1,2] refrigeration cycles[2], microelectronic cooling[3] and a novel field of nanofluidic biochips[4], a controlled method of heat dissipation is paramount if these processes are to function properly. As elevated heat dissipation and thermal management present obstacles to the optimization and sizing of nano-scale devices [5], sensible heat transfer using single phase cooling has proven to be ineffective [6]. Owing to the latent heat of vaporization involved in the case of phase change heat transfer, such mechanisms of heat dissipation have proven to be more efficient compared to their sensible counterparts [7]. Such a process of latent heat transfer is condensation, a phenomenon in which a matter transforms form its vapor phase to its liquid phase, visible when a liquid condensate starts to precipitate on the surface of the substrate [8] The condensation

process is a crucial element of phase-change cooling systems, playing a significant role even in common devices like mobile phones and laptops that use heat pipes to cool the CPU. The cooling mechanism primarily involves the transfer of heat from a high-temperature vapor to a liquid coolant, which is typically separated from the vapor by a solid conductive surface. Heat is first conducted through this surface and then passed on to the coolant. This heat removal creates a temperature gradient, resulting in the vapor near the wall reaching its lowest temperature.[9]

Over the years, researchers have studied condensation of molecules as a phenomenon occurring in the nanoscale. Various modifications have been made to the substrate so that the heat transfer characteristics are maximized. The surface modifications are primarily made in terms of wettability and design [10]. Condensation occurs on solid surfaces in two distinct mechanism – filmwise condensation (FWC) and dropwise condensation (DWC). Various arrangements of the surface wettability have been studied to provide the optimum wettability contrast for optimized condensation of any of the above two types. Generally, FWC is supported by hydrophilic surfaces because of the higher nucleation density, and DWC by hydrophobic surfaces because of the finer droplet removal [11–14]. Heat transfer rates are maximized by utilizing the synergy between these two effects, by carrying out condensation studies on hybrid wetting surfaces. Such surfaces contain varying strengths of hydrophobicity and hydrophilicity achieved through chemical treatment[15–17], micro/nano-structure morphology design[18–21] and others.

Over the last decade, Molecular Dynamics (MD) simulations have come as quite a handy tool to researchers in studying the condensation process in nanoscale, as several factors concerning the heat transfer can be identified and discerned, including the combination various wetting conditions and solid-liquid interactions at the interface. Paul et al.[22] studied nanoscale condensation heat transfer on two types hybrid wetting surfaces – patterned and Functionally Gradient Wettability (FGW) surfaces, and found that for both cases, the condensation heat transfer is optimum when hydrophilicity is stronger and hydrophobicity is weaker. Another method of surface modification is surface topological morphology. MD simulations have been extensively used to observe the effect of surface topology modification on phase change heat transfer. Li et al. [23] showed that the addition of cuboid nanostructures to the condensing surface facilitated condensation heat transfer due to increased surface area and the increased distance between the nanostructure surface and cold end. Morshed et al. [24]showed the same for boiling heat transfer – the evaporation rate of argon increased with the presence of nanostructures on the surface. Furthermore, Ghahremanian et al. [25] found that nanostructure obtained using Green-Kubo relations showed enhanced energy transfer during initial condensation.

Most of the research mentioned above make use of simple nano-structure geometry, with a handful of studies conducted on surfaces involving complex topological configurations. Song et al. [26] made use of MD simulations to understand convection heat transfer characteristics of nanochannels with complex surface topological morphology. Superimposed sinusoidal functions were used to provide the rough surface structure, and the results showed an enhanced heat transfer as the number of superimposed sine functions was increased. Using superimposed sinusoidal functions to model complex surface geometry could help us achieve two things Firstly, we can better understand the roughness patterns of already existing surfaces (natural or synthetic) by applying Fourier transform to study their properties. Secondly, we can obtain and manufacture surfaces optimized for enhanced condensation heat transfer in the form of equations that make the surface easy to manufacture via methods such as additive or subtractive manufacturing. Although superimposed sinusoidal functions were used to study convection heat transfer, only simple nanostructures are studied for condensation. Thus, this work addresses the gap by proposing a molecular dynamics study of Ar atoms condensing on a series of rough surfaces having topological configurations of superimposed sinusoidal functions. The condensing surface has a FGW – governed hydrophilic-hydrophobic composition. The work compares the effect of the order of the sine functions in enhancing the condensation heat transfer.

PROBLEM STATEMENT AND SOLUTION METHODOLOGY

Simulation Model

The simulation domain was created using an input script for the Large-scale Atomic/Molecular Massively Parallel Simulator (LAMMPS). As depicted in Figure 1, the setup includes two solid platinum (Pt) substrates and a fluid sample consisting of pure argon (Ar). The platinum substrates, with a density of 21,450 kg/m³, are arranged in a face-centered cubic (FCC) (1 0 0) lattice and are positioned at the top and bottom of the simulation domain. The bottom platinum substrate is flat and supports a 4 nm-thick layer of liquid argon with a density of 1378 kg/m³ at 90 K. The remaining

space between the substrates is filled with saturated argon vapor at 90 K, with a density of 6.751 kg/m³. To ensure system stability, the forces and velocity components of atoms in the bottommost layer are set to zero, preventing atoms from leaving the domain. The next two layers act as phantom atoms and serve as the heat source, while the following five layers conduct heat to the argon atoms on the bottom substrate. The top platinum substrate mirrors these atomistic properties. At the beginning of the simulation, the system contained 26,586 Pt atoms, 10,395 liquid Ar atoms, and 1,336 vapor Ar atoms, all organized in their respective FCC crystal structures. Periodic boundary conditions were applied along the *x* and *z* axes, while a fixed boundary condition was used along the *y* axis. This simulation models a Lennard-Jones (L-J) system, employing the 12-6 L-J potential to calculate intermolecular interactions. The intermolecular potential, ϕ, is defined by Eq. (1).

$$\phi = 4\varepsilon_{ij}\left[\left(\frac{\sigma_{ij}}{r_{ij}}\right)^{12} - \left(\frac{\sigma_{ij}}{r_{ij}}\right)^{6}\right] \text{ for, } r_{ij} < r_{cut} \quad \text{i)}$$

$$\phi = 0 \quad \text{for, } r_{ij} < r_{cut} \quad \text{ii)}$$

Here, ε_{ij} represents the depth of the potential well, σ_{ij} represents the distance where the interparticle potential is zero, and r_{ij} is the distance between the two atoms. A cutoff distance, r_{cut}, of 4.5σAr-Ar is chosen for the improvement of the computational performance. The literature values [27,28] of the length parameters and potential well depths of the system are listed in the TABLE 1. The altered magnitudes of depth of potential well for the hydrophilic and hydrophobic platinum atoms and the argon atoms were achieved with the approach of Hens et al. [29]

$\varepsilon_{Ar\text{-}Pt}$ is found to be 0.0208 eV for hydrophilic platinum and 0.0052 for hydrophobic platinum.

TABLE 1. LJ model parameters for Ar and Pt.

Atom	ε (eV)	σ (nm)
Ar	0.0104	0.3405
Pt	0.5211	0.2475

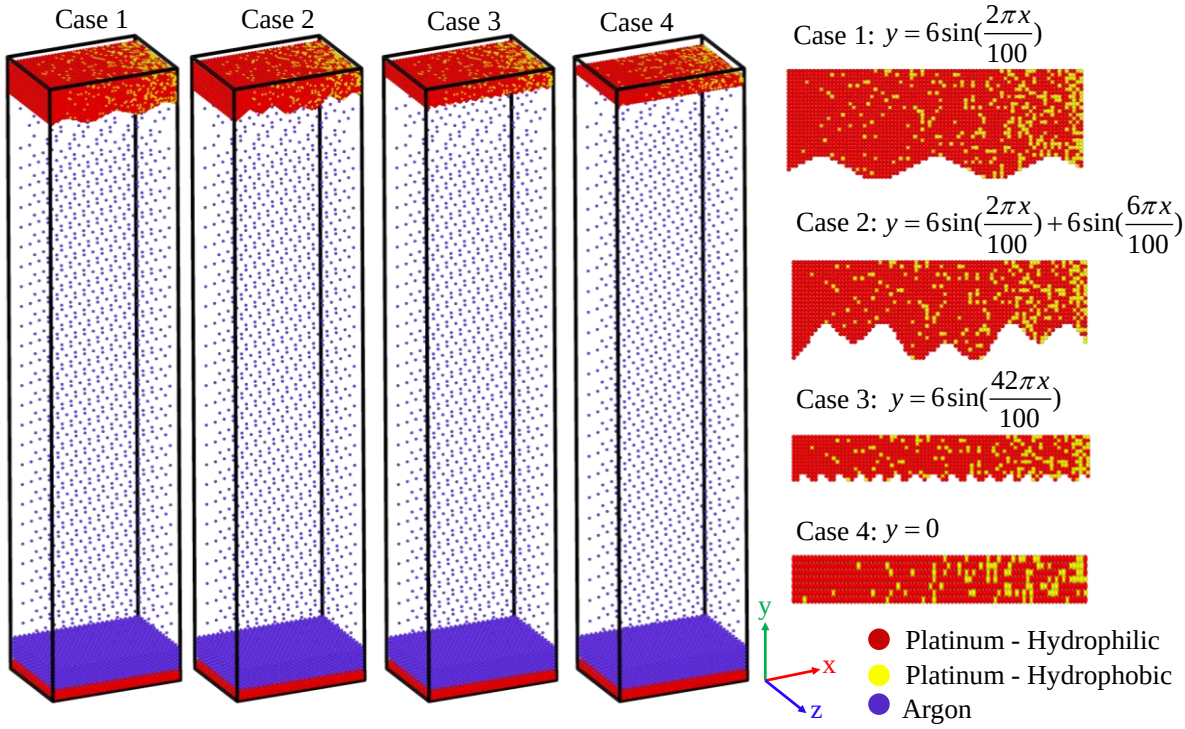

FIGURE 1. ADD caption

Modeling of FGW and rough wetting surfaces

To model the effect of surface roughness on different configurations of hybrid wetting surfaces, sinusoidal functions have been used to define the surface structure, maintaining a fixed 84% hydrophilic surface coverage. In alignment with the methodology outlined by **Paul et al.**,[30] the entire solid substrate within the specified dimensions is substituted with hydrophilic atoms. The roughness pattern is introduced by cutting off sinusoidal features from the *X*- and *Y*-axes of the solid substrate. These sinusoidal functions are defined mathematically to represent nanoscale surface structuring, which influences the wetting properties. The input scripts required for this model are generated using the **nanoHUB tool**, which allows for precise surface manipulation. FIGURE 1 demonstrates the initialized models, showcasing the superimposed surface structures. The sinusoidal roughness is described mathematically for both the *X*- and *Y*-directions, reflecting the nanostructured features of the surfaces.

Simulation procedure

The simulation process in this study is divided into two stages: equilibrium molecular dynamics (EMD) and non-equilibrium molecular dynamics (NEMD). In the EMD stage, the system is run using the canonical ensemble for 0.5 ns, with the temperature maintained at 90 K by a Langevin thermostat. Figure 2 illustrates the trend in potential energy over time during equilibration for different cases. As the system equilibrates, the potential energy decreases gradually before stabilizing, a behavior observed consistently across all four cases. After achieving thermal equilibrium, the non-equilibrium molecular dynamics (NEMD) session began, conducted under the microcanonical ensemble for 2.0 ns. In this phase, the temperatures of the phantom atoms in the upper and lower substrates were set to 130 K and 90 K, respectively, controlled by a Langevin thermostat.

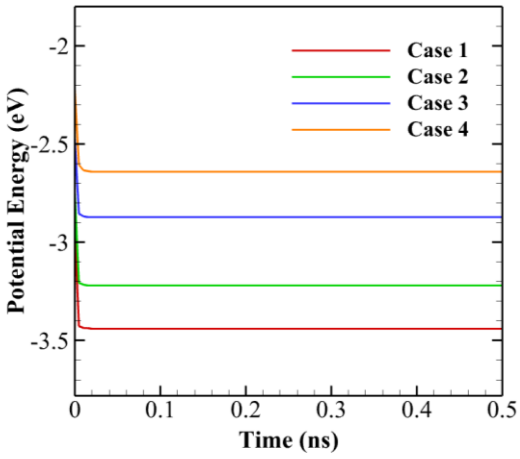

FIGURE 2. Variation of system potential energy during equilibration simulation

During the NEMD process, liquid atoms absorbed thermal energy from the lower substrate, leading to evaporation. These atoms then released energy to the upper substrate, undergoing condensation. The lower substrate emulated the evaporating surface, while the upper substrate simulated the condensing surface. To ensure the condensing surface's performance remained unaffected by the evaporation process, the wetting behavior of the evaporating surface was kept constant with a value of $\varepsilon r = 2$ across all cases. The NEMD session lasted 6.6 ns, with the positions and velocities of atoms determined using Newton's equations of motion. A velocity-Verlet algorithm, with a timestep of 5 fs, was applied to solve these equations. Visualization of atomic trajectories was generated using OVITO software.

RESULTS AND DISCUSSION

This section will illustrate the condensation characteristics of different hybrid wetting surfaces for all the cases considered in this work. The condensation attributes of all the surfaces are evaluated by assessing the important metrics used in the molecular dynamics analysis of condensation process, e.g., system characteristics, nucleation, coalescence,

and growth mode of the condensates, number of atoms condensed, mass flux during condensation, and condensing surface heat flux. T

Time history of system behavior

The temporal evolution of the total energy of argon atoms for all considered cases is presented in Fig. [X]. In the initial phase, from 0.25 ns to 0.5 ns, the total energy across all cases is approximately -0.06 eV per atom, indicating relatively uniform interactions between the argon atoms and the platinum substrate, irrespective of surface roughness. This validates that the system has reached thermal equilibrium in the first 0.5 ns.

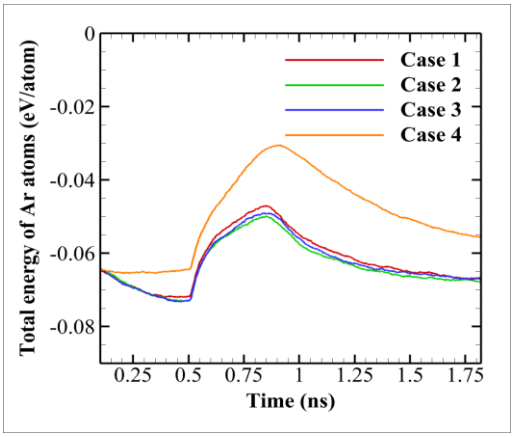

FIGURE 2. Variation of system potential energy during equilibration simulation

During the time interval between 0.5 ns and 1.0 ns, a general upward trend in total energy is observed. Notably, Case 4 (smooth surface) exhibits the least negative energy peak, reaching approximately -0.02 eV per atom. This increase in energy corresponds to dynamic processes such as condensation and adsorption. The smoother surface in Case 4 is associated with weaker atom-surface interactions, resulting in a less stable system, as reflected by the higher (less negative) energy values compared to the rougher surfaces. In contrast, Cases 1, 2, and 3, characterized by rougher surfaces, demonstrate more negative energy peaks, indicative of stronger atom-surface interactions, thereby conferring greater stability to the system through enhanced energy dissipation.

Beyond 1.0 ns, the total energy begins to decrease, and by 1.5 ns, all cases approach a more stable energetic state. However, Case 4 exhibits a slower stabilization process, maintaining higher (less negative) energy for a prolonged duration, which is indicative of reduced stability on the smooth surface. Conversely, Cases 1, 2, and 3, with increased surface roughness, stabilize more rapidly and at lower (more negative) energy levels. This behavior suggests that increased surface roughness enhances system stability by facilitating more frequent and complex interactions between the argon atoms and the surface, thereby promoting greater energy dissipation.

These findings underscore the pivotal role of surface roughness in influencing the stability of argon atoms. Rougher surfaces lead to more negative total energy values, reflecting stronger interactions and greater system stability, whereas smoother surfaces, as seen in Case 4, exhibit less negative energy over time, indicating lower stability.

Condensate nucleation, coalescence and growth characteristics

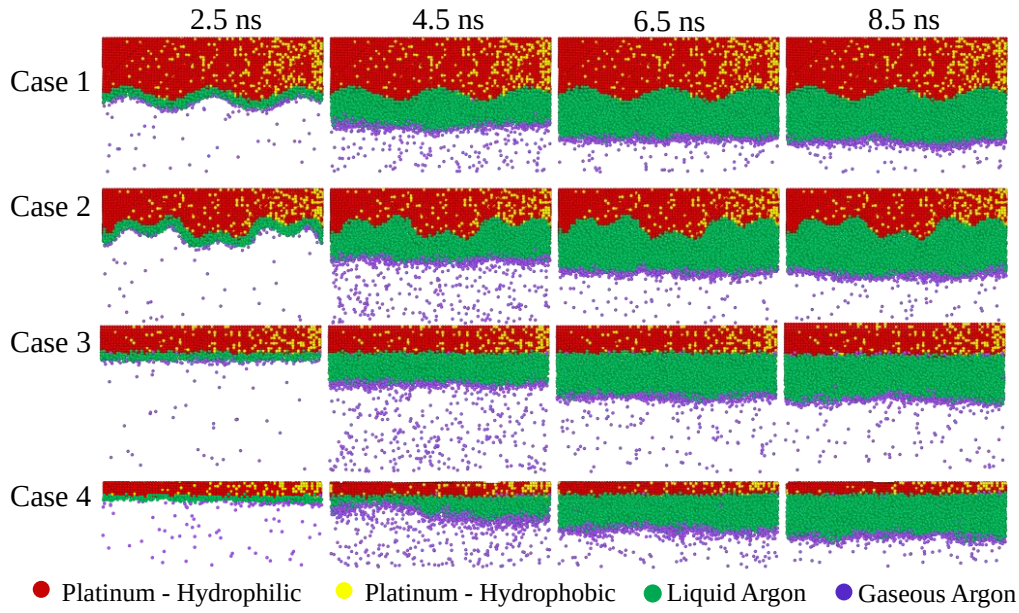

FIGURE 2. Variation of system potential energy during equilibration simulation

The presence of surface roughness, especially in cases 1 and 2 with multiple sinusoidal components, leads to enhanced nucleation sites. This behavior is due to the interplay between the hydrophilic and hydrophobic regions. The hydrophilic platinum regions (red) are more prone to attracting condensate atoms, resulting in initial cluster formations at these sites. Over time, these clusters serve as seeding points, encouraging further condensation as seen by the dense population of green (liquid) and purple (vapor) Ar atoms near these regions. The rougher surfaces, particularly in case 3 (high-frequency roughness), exhibit a larger number of initial clusters. This behavior is evident from the first few nanoseconds, where there is a rapid increase in the number of surface clusters, as shown in the **figure 2**. As time progresses, these clusters tend to stabilize, resulting in coalescence and growth. In **figure 3**, which shows the number of surface clusters over time, indicates that surfaces with higher roughness (e.g., case 3) maintain a higher number of clusters, especially during the early stages. The number of clusters peaks quickly, indicating rapid nucleation. However, these clusters do not persist indefinitely; they coalesce and reduce in number as the simulation progresses, leading to larger but fewer clusters. As condensation proceeds, individual clusters begin to merge, forming larger liquid droplets. The surface roughness significantly influences this coalescence. For case 2, the coalescence occurs in a more distributed manner, with clusters merging along the sinusoidal valleys. This results in a uniform spread of the liquid phase. The growth of condensation clusters depends on the distribution of surface features. In case 3, the growth is localized, with clusters rapidly filling the valleys and creating larger droplets along these regions. For smoother surfaces in case 4, the growth is more isotropic, and the clusters spread uniformly across the surface. The interplay between hydrophilic and hydrophobic regions creates an uneven energy landscape, which affects how clusters grow. Hydrophilic regions promote rapid condensation, while hydrophobic regions hinder it, leading to differential growth rates. This behavior can be observed in the cluster density variations across different cases.

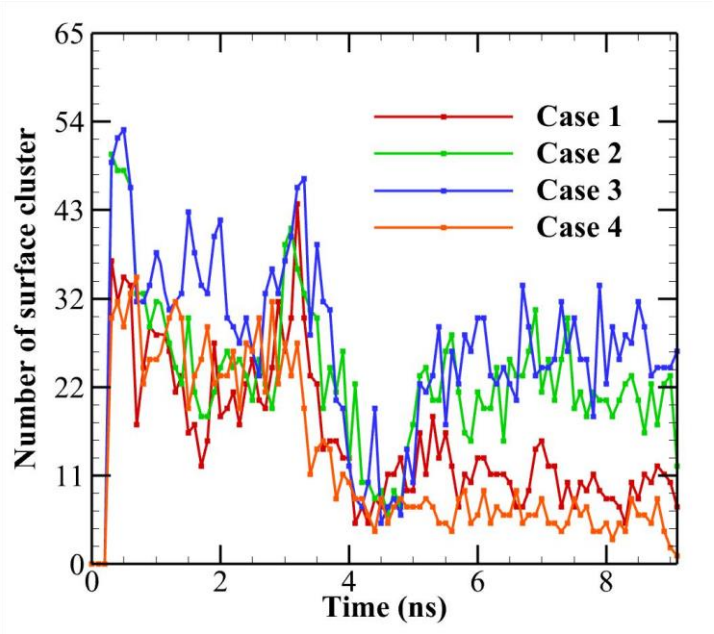

FIGURE 2. Variation of system potential energy during equilibration simulation

From Figure 3, it can be seen that surfaces with high roughness (e.g., case 3) tend to have a higher initial cluster count. However, as time progresses, the cluster count decreases, indicating that these clusters are merging into larger ones. Case 1 and Case 4 show lower initial cluster counts and a relatively stable cluster number over time. This suggests that the lack of pronounced roughness leads to slower nucleation rates and less dynamic cluster merging behavior. Case 2 and Case 3 exhibit more fluctuations in cluster count, with case 3 showing the highest initial cluster count. The high-frequency sinusoidal surface in case 3 provides numerous nucleation sites, resulting in rapid initial growth and subsequent cluster coalescence. The overall number of condensed atoms is directly related to surface roughness. Rougher surfaces tend to attract more condensation atoms, as they offer more nucleation sites due to the increased surface area. As the condensation process progresses, the atoms tend to move toward regions of higher curvature (i.e., the valleys in the sinusoidal surfaces). This leads to localized condensation and clustering, as observed in cases 1 and 2. In contrast, for smoother surfaces (case 4), the condensation atoms distribute more evenly across the surface, leading to a more uniform growth pattern. The total number of condensation atoms on such surfaces remains lower compared to rougher surfaces, highlighting the significant role of surface morphology in condensation behavior.

The number density changes of argon atoms at are shown in Fig. 6. It can be seen that all cases have the non-evaporated layers, but the number density profiles of these layers are different.

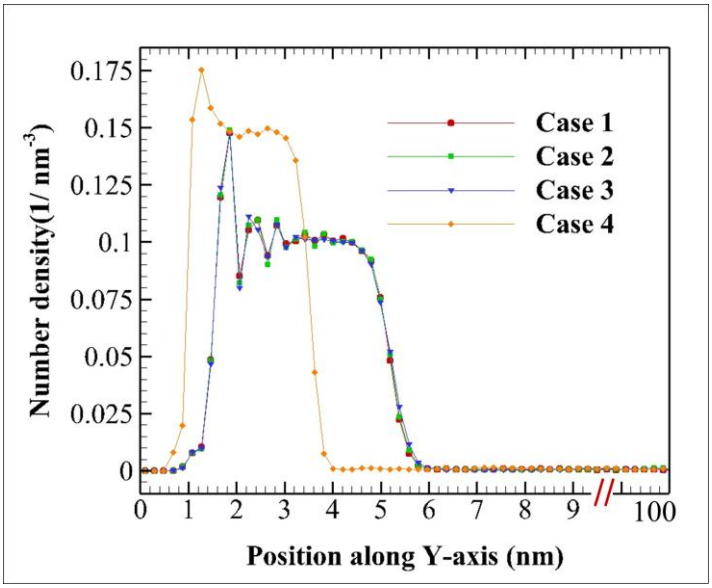

FIGURE 2. Variation of system potential energy during equilibration simulation (add a paragraph on this)

Condensation performance at different rough configurations

To evaluate the condensation performance of the four surfaces, the number of condensed atoms on the upper surface was tracked and analyzed at each timestep. The data, as shown in Fig. clearly demonstrate that Case 2, with the highest surface roughness as demonstrated by its mathematical expression, exhibited the greatest number of condensed atoms. This suggests that surface roughness plays a crucial role in enhancing condensation, as in all the four cases, the upper surfaces have an equal hydrophilic fraction of 84 %.

When comparing the other cases, the total number of condensed atoms follows the order **Case 1** > **Case 3** > **Case 4**. **Case 1**, while slightly less rough than **Case 2**, still demonstrated a higher number of condensed atoms compared to **Cases 3** and **4**. The difference between **Case 1** and **Case 2** is subtle, indicating that even small variations in roughness can lead to significant changes in condensation behavior. This finding suggests that moderate roughness can still enhance condensation performance, potentially due to effective droplet retention and coalescence. In contrast, **Cases 3** and **4**, with lower roughness values, showed reduced condensation capabilities, highlighting the detrimental impact of smooth surfaces on condensation efficiency. As seen in Fig. 13, the difference in the number of condensed atoms across the cases tends to diminish when the surfaces have more uniform roughness profiles. This suggests that roughness plays a more dominant role when there are significant variations in surface topology.

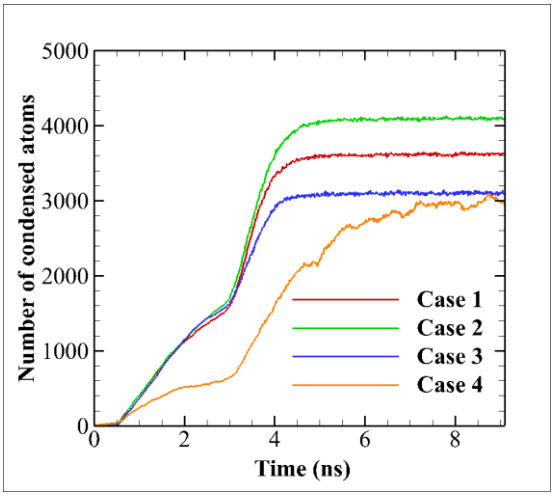

FIGURE . Time history of condensation of argon atoms

The rate of condensation was also evaluated by calculating the condensation mass flux which is obtained by the instantaneous slope of the curves from Fig . The results, shown in Fig. follow a trend similar to the number of condensed atoms. Surfaces with greater roughness, particularly **Case 2**, exhibit higher condensation mass flux values, indicating better heat transfer performance. The sequence of condensation rates follows the same order: **Case 2 > Case 1 > Case 3 > Case 4**.

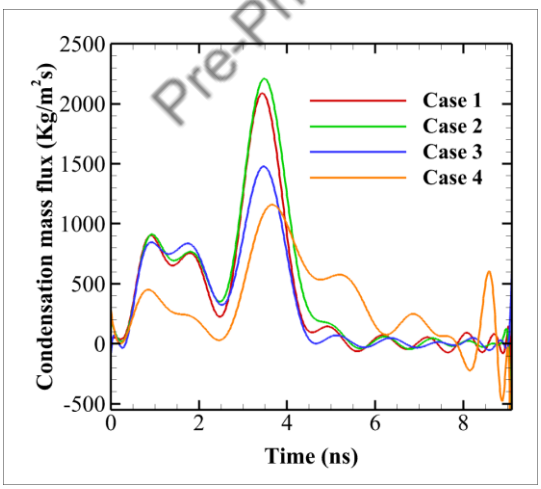

FIGURE . Time history of condensates' mass flux

These findings highlight the importance of surface roughness in improving condensation rates and heat transfer performance. With the hydrophilic fraction held constant, rougher surfaces consistently show superior condensation characteristics, confirming the critical role that roughness plays in such processes.
The radial distribution function for all the elements in all four cases are shown in Fig. X.

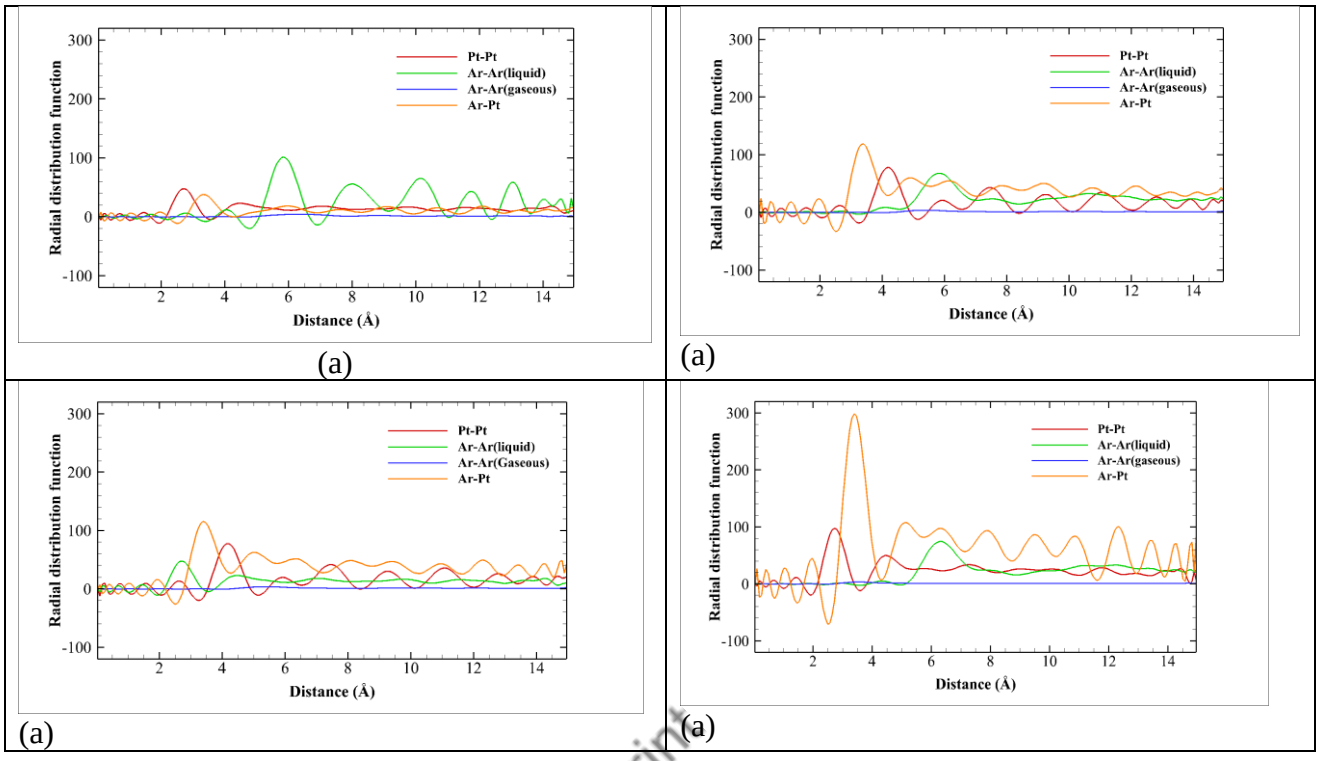

FIGURE . Time history of condensates' mass flux

The temperature profile across various y-coordinates demonstrated in Fig. exhibits fluctuations between **90 K** and **130 K**, reflecting the dynamic molecular motion during phase changes, particularly evaporation and condensation. As molecules undergo phase changes, they absorb or release latent heat, resulting in localized heating or cooling.

This process leads to peaks in the temperature profile, especially in regions of intense condensation.

In molecular dynamics (MD) simulations, the temperature is closely related to the average kinetic energy of the molecules within specific regions. Increased molecular collisions in certain areas result in higher kinetic energy, thereby elevating temperatures. Conversely, in regions where molecular motion slows down due to clustering or phase transitions, temperatures decrease. The role of intermolecular forces, particularly van der Waals interactions, is critical at the interfaces between different phases, influencing molecular behavior and leading to significant temperature fluctuations.

Interfacial thermal resistance, arising from differences in electrostatic and vibrational properties at the interfaces of dissimilar phases, contributes to temperature jumps. In this context, case 2 exhibits lower temperature fluctuations compared to case 1, which is slightly smoother but possesses greater surface area interactions that lead to increased fluctuations. Case 3, characterized by a high-frequency surface texture that closely mimics a flat surface,

demonstrates fluctuations akin to case 4, which shows the highest fluctuations due to its inability to promote efficient heat transfer.

Moreover, in systems characterized by alternating cycles of evaporation and condensation, distinct temperature gradients emerge. Molecules in the gas phase generally have higher kinetic energy, resulting in elevated temperatures compared to their condensed counterparts in the liquid phase. This temperature disparity creates observable variations along the column, reflecting the intricate balance between evaporation and condensation processes. Overall, the fluctuations observed between **90 K** and **130 K** underscore the complexities and significance of phase change heat transfer in thermal management applications.

Heat flux characteristics across the condensing wall

The condensing surface heat flux, is calculated to quantify the rate at which heat is extracted from fluid atoms during the phase change process. The results presented in Fig. demonstrate that the maximum heat flux values follow the order: **Case 2 > Case 1 > Case 3 > Case 4** across all surfaces analyzed. This trend aligns with the condensation mass flux observed in earlier sections, highlighting the influence of surface characteristics on thermal performance.
Despite maintaining an equal hydrophilic fraction of **84%** across all cases, the variation in surface roughness significantly impacts the heat flux characteristics. Specifically, **Case 2**, with its enhanced roughness, achieves the highest maximum condensing wall heat flux, indicative of its superior heat transfer capability. Conversely, **Case 4**, despite having lower roughness, exhibits the least effective heat flux performance, which can be attributed to its smoother surface structure.

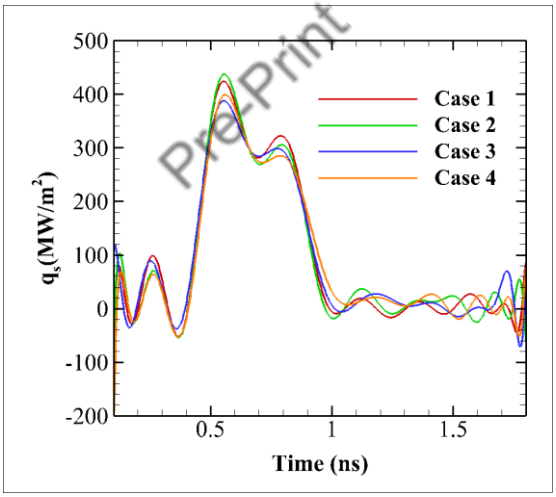

FIGURE . Time history of condensing surface heat flux

As demonstrated by the plot, the trends observed across all four cases remain consistent, with each case exhibiting a transient nature in the heat flux characteristics. The differences in average heat flux values are relatively small, primarily attributed to the variations in surface roughness. However, no significant difference in the overall trend is noted, as all cases maintain the same hydrophilic fraction of **84%**. This consistency emphasizes that while surface roughness plays a role in influencing heat transfer performance, the fundamental trend remains stable across different configurations.
In conclusion, the analysis confirms that the heat flux performance of the surfaces is significantly influenced by surface roughness, with greater roughness correlating with enhanced condensation characteristics. Thus, optimizing surface roughness is crucial for improving heat transfer efficiency in applications involving phase change processes.

.

CONCLUSION

In this section we welcome you to include a summary of the end results of your research. Font should be Times New Roman, 10 pt.

ACKNOWLEDGMENTS

We want to thank ASHRAE BUET Student Chapter for providing computational support. [Improve this]

REFERENCES

[1] J.M. Beér, "High efficiency electric power generation: The environmental role," Prog Energy Combust Sci **33**(2), 107–134 (2007).
[2] M.-H. Kim, and C.W. Bullard, *Air-Side Performance of Brazed Aluminum Heat Exchangers under Dehumidifying Conditions* (n.d.).
[3] N.V. Upot, K. Fazle Rabbi, S. Khodakarami, J.Y. Ho, J. Kohler Mendizabal, and N. Miljkovic, "Advances in micro and nanoengineered surfaces for enhancing boiling and condensation heat transfer: a review," Nanoscale Adv **5**(5), 1232–1270 (2022).
[4] D. Xia, J. Yan, and S. Hou, "Fabrication of nanofluidic biochips with nanochannels for applications in DNA analysis," Small **8**(18), 2787–2801 (2012).
[5] D. Vasileska, "Modeling thermal effects in nano-devices," Microelectron Eng **109**, 163–167 (2013).
[6] G. Liang, Y. Chen, H. Yang, D. Li, and S. Shen, "Nucleate boiling heat transfer and critical heat flux (CHF) from micro-pit surfaces," Int J Heat Mass Transf **152**, (2020).
[7] B. Agostini, J.R. Thome, M. Fabbri, and B. Michel, "High heat flux two-phase cooling in silicon multimicrochannels," IEEE Transactions on Components and Packaging Technologies **31**(3), 691–701 (2008).
[8] W.M.. Rohsenow, J.P.. Hartnett, and Y.I.. Cho, *Handbook of Heat Transfer* (McGraw-Hill, 1998).
[9] A. Goswami, S.C. Pillai, and G. McGranaghan, "Surface modifications to enhance dropwise condensation," Surfaces and Interfaces **25**, (2021).
[10] S. Qin, R. Ji, C. Miao, L. Jin, C. Yang, and X. Meng, "Review of enhancing boiling and condensation heat transfer: Surface modification," Renewable and Sustainable Energy Reviews **189**, (2024).
[11] N. Miljkovic, R. Xiao, D.J. Preston, R. Enright, I. McKay, and E.N. Wang, "Condensation on hydrophilic, hydrophobic, nanostructured superhydrophobic and oil-infused surfaces," J Heat Transfer **135**(8), 1 (2013).
[12] A. Starostin, V. Valtsifer, Z. Barkay, I. Legchenkova, V. Danchuk, and E. Bormashenko, "Drop-wise and film-wise water condensation processes occurring on metallic micro-scaled surfaces," Appl Surf Sci **444**, 604–609 (2018).
[13] S. Daniel, M.K. Chaudhury, and J.C. Chen, "Fast drop movements resulting from the phase change on a gradient surface," Science (1979) **291**(5504), 633–636 (2001).
[14] C. Dorrer, and J. Rühe, "Some thoughts on superhydrophobic wetting," Soft Matter **5**(1), 51–61 (2009).

[15] M.M. Derby, A. Chatterjee, Y. Peles, and M.K. Jensen, “Flow condensation heat transfer enhancement in a mini-channel with hydrophobic and hydrophilic patterns,” Int J Heat Mass Transf **68**, 151–160 (2014).
[16] B. Peng, X. Ma, Z. Lan, W. Xu, and R. Wen, “Experimental investigation on steam condensation heat transfer enhancement with vertically patterned hydrophobic-hydrophilic hybrid surfaces,” Int J Heat Mass Transf **83**, 27–38 (2015).
[17] K. Egab, M. Alwazzan, B. Peng, S.K. Oudah, Z. Guo, X. Dai, J. Khan, and C. Li, “Enhancing filmwise and dropwise condensation using a hybrid wettability contrast mechanism: Circular patterns,” Int J Heat Mass Transf **154**, (2020).
[18] X. Chen, J. Wu, R. Ma, M. Hua, N. Koratkar, S. Yao, and Z. Wang, “Nanograssed micropyramidal architectures for continuous dropwise condensation,” Adv Funct Mater **21**(24), 4617–4623 (2011).
[19] C.W. Lo, C.C. Wang, and M.C. Lu, “Spatial control of heterogeneous nucleation on the Superhydrophobic Nanowire Array,” Adv Funct Mater **24**(9), 1211–1217 (2014).
[20] A. Tokunaga, and T. Tsuruta, “Enhancement of condensation heat transfer on a microstructured surface with wettability gradient,” Int J Heat Mass Transf **156**, (2020).
[21] B. Mondal, M. Mac Giolla Eain, Q.F. Xu, V.M. Egan, J. Punch, and A.M. Lyons, “Design and Fabrication of a Hybrid Superhydrophobic-Hydrophilic Surface That Exhibits Stable Dropwise Condensation,” ACS Appl Mater Interfaces **7**(42), 23575–23588 (2015).
[22] S. Paul, D. Chakraborty, S.J. Esha, and M.N. Hasan, “Role of wettability contrast on nanoscale condensation over hybrid wetting surface with gradient and patterned wetting configuration at various philic-phobic content,” Surfaces and Interfaces **36**, (2023).
[23] L. Li, P. Ji, and Y. Zhang, “Molecular dynamics simulation of condensation on nanostructured surface in a confined space,” Appl Phys A Mater Sci Process **122**(5), (2016).
[24] A.K.M.M. Morshed, T.C. Paul, and J.A. Khan, “Effect of nanostructures on evaporation and explosive boiling of thin liquid films: A molecular dynamics study,” Appl Phys A Mater Sci Process **105**(2), 445–451 (2011).
[25] S. Ghahremanian, A. Abbassi, Z. Mansoori, and D. Toghraie, “Effect of nanostructured surface configuration on the interface properties and heat transfer of condensation process of argon inside nanochannels using molecular dynamics simulation,” J Mol Liq **339**, 117281 (2021).
[26] Z. Song, Z. Cui, Y. Liu, and Q. Cao, “Heat transfer and flow characteristics in nanochannels with complex surface topological morphology,” Appl Therm Eng **201**, (2022).
[27] S.C. Maroo, and J.N. Chung, “Molecular dynamic simulation of platinum heater and associated nano-scale liquid argon film evaporation and colloidal adsorption characteristics,” J Colloid Interface Sci **328**(1), 134–146 (2008).
[28] A.K.M.M. Morshed, T.C. Paul, and J.A. Khan, “Effect of nanostructures on evaporation and explosive boiling of thin liquid films: A molecular dynamics study,” Appl Phys A Mater Sci Process **105**(2), 445–451 (2011).
[29] A. Hens, R. Agarwal, and G. Biswas, “Nanoscale study of boiling and evaporation in a liquid Ar film on a Pt heater using molecular dynamics simulation,” Int J Heat Mass Transf **71**, 303–312 (2014).
[30] S. Paul, D. Chakraborty, S.J. Esha, and M.N. Hasan, “Role of wettability contrast on nanoscale condensation over hybrid wetting surface with gradient and patterned wetting configuration at various philic-phobic content,” Surfaces and Interfaces **36**, (2023).
1.